Structure of the hydrated Ca2+ and Cl−: Combined X-ray absorption measurements and QM/MM MD simulations study

ARTICLE *in* PHYSICAL CHEMISTRY CHEMICAL PHYSICS · SEPTEMBER 2010

Impact Factor: 4.49 · DOI: 10.1039/c0cp00136h · Source: PubMed

4 AUTHORS, INCLUDING:

Saroj Rujirawat
Suranaree University of Technology
67 PUBLICATIONS **581** CITATIONS
SEE PROFILE

Sukit Limpijumnong
Suranaree University of Technology
128 PUBLICATIONS **3,510** CITATIONS
SEE PROFILE

Structure of the hydrated Ca^{2+} and Cl^{-}: Combined X-ray absorption measurements and QM/MM MD simulations study

Anan Tongraar,*[a] Jiraroj T-Thienprasert,[bc] Saroj Rujirawat[cd] and Sukit Limpijumnong[cd]

Received 6th April 2010, Accepted 28th May 2010
DOI: 10.1039/c0cp00136h

A combination of X-ray absorption spectroscopy (XAS) measurements and quantum mechanical/molecular mechanical (QM/MM) molecular dynamics (MD) simulations has been applied to elucidate detailed information on the hydration structures of Ca^{2+} and Cl^{-}. The XAS spectra (extended X-ray absorption fine structure, EXAFS, and X-ray absorption near-edge structure, XANES) measured from aqueous $CaCl_2$ solution were analyzed and compared to those generated from snapshots of QM/MM MD simulations of Ca^{2+} and Cl^{-} in water. With regard to this scheme, the simulated QM/MM–EXAFS and QM/MM–XANES spectra, which correspond to the local structure and geometrical arrangement of the hydrated Ca^{2+} and Cl^{-} at molecular level show good agreement with the experimentally observed EXAFS and XANES spectra. From the analyses of the simulated QM/MM–EXAFS spectra, the hydration numbers for Ca^{2+} and Cl^{-} were found to be 7.1 ± 0.7 and 5.1 ± 1.3, respectively, compared to the corresponding values of 6.9 ± 0.7 and 6.0 ± 1.7 derived from the measured EXAFS data. In particular for XANES results, it is found that ensemble averages derived from the QM/MM MD simulations can provide reliable QM/MM–XANES spectra, which are strongly related to the shape of the experimental XANES spectra. Since there is no direct way to convert the measured XANES spectrum into details relating to geometrical arrangement of the hydrated ions, it is demonstrated that such a combined technique of XAS experiments and QM/MM MD simulations is well-suited for the structural verification of aqueous ionic solutions.

1. Introduction

The characteristics of ions solvated in polar solvents, in particular water, have long been a topic of scientific interest in order to understand the role of these ions in chemical and biological processes.[1,2] In general, such detailed knowledge can be obtained from a variety of experimental and theoretical techniques. In experiments, powerful techniques from a structural viewpoint are neutron and X-ray diffraction because they offer a direct probe of the ionic structure.[3–9] However, especially for multi-component systems, discrepancies in the established data exist, even for fundamental properties such as the mean ion–oxygen nearest-neighbor distance and the average number of coordinating solvent molecules. Some explicit reasons are due to the uncertainty in modeling the scattering data as well as to the lack of direct information relating to the static and dynamics properties of solvent molecules surrounding the ions.

Besides the diffraction techniques, X-ray absorption spectroscopy (XAS) is a powerful tool for an accurate structural determination of solvated ions, because of its element selectivity. In addition, since most of the diffraction techniques restrict their use only for relatively high concentrations, the XAS technique can be applied to a wider range of concentrated solutions. With respect to the XAS analysis, the spectra have been subdivided into a high-energy region (50–1000 eV), termed extended X-ray absorption fine structure (EXAFS), and a low-energy region (0–50 eV), which is called X-ray absorption near-edge structure (XANES). For relatively large disordered systems, like aqueous ionic solutions, the EXAFS spectra can provide a good resolution in detecting a near-neighbor solvent environment, especially for systems with a high degree of local order, while the XANES spectra correspond to the geometrical arrangement of the solvated ions. However, it is known that the presence of multiple scattering (MS) effects[10,11] in the spectra as well as the errors from asymmetric distributions[12,13] are major problems in the analysis of XAS data. To simplify the process of XAS data analysis and interpretation, the use of information derived from other sources, such as molecular simulations, is of special interest.

Molecular simulations, in particular the molecular dynamics (MD) technique, have been employed to generate partial pair distributions, $g(R)$'s, from which a model $\chi(k)$ is constructed and then used as a starting model in the analysis of XAS data. In this respect, the accuracy in the XAS data analysis depends crucially on the quality of the simulation results, *i.e.*, the reliability of the ensemble averages. The combined XAS

[a] *School of Chemistry, Institute of Science, Suranaree University of Technology, Nakhon Ratchasima 30000, Thailand*
[b] *Department of Physics, Faculty of Science, Kasetsart University, Bangkok 10900, Thailand*
[c] *Thailand Center of Excellence in Physics (ThEP Center), Commission on Higher Education, Bangkok 10400, Thailand*
[d] *School of Physics, Institute of Science, Suranaree University of Technology, and Synchrotron Light Research Institute, Nakhon Ratchasima 30000, Thailand*

measurements, in particular EXAFS, and the MD simulations technique have been successfully applied to several aqueous and non-aqueous ionic solutions, providing a more comprehensive understanding of the structural properties of solvated ions.[13–25] By this scheme, however, the detailed information derived from molecular simulations relies mostly on molecular mechanical (MM) force fields, *i.e.*, the potential functions describing the ion–water and water–water interactions are usually constructed with respect to a set of experimental data or to *ab initio* calculations. For strong interacting systems, like aqueous ionic solutions, it has been demonstrated that "quantum effects" are significant and that the inclusion of these effects in the simulations is mandatory.[26,27] Nowadays, a high-level quantum mechanics/molecular mechanics (QM/MM) MD technique has been shown to be an elegant approach for studying condensed-phase systems, in particular the aqueous ionic solutions.[26–36] With regard to the QM/MM MD technique, the most interesting region, a sphere which includes the ion and its surrounding solvent molecules, is treated quantum mechanically. As a result, the complicated many-body contributions as well as the polarization effects, which are hardly accessible through the basic assumptions underlying the MM potentials, can be reliably included into the defined QM region.

Consequently, the aim of this study is to apply a combined technique of XAS (EXAFS and XANES) measurements and high-accuracy QM/MM MD simulations for studying the hydration shell structure of Ca^{2+} and Cl^{-}. For Ca^{2+}, established results in the literature, both experimental and theoretical investigations, reveal a rather inhomogeneous picture of this hydrated ion. X-Ray diffraction (XRD) experiments on calcium halide aqueous solutions reported hydration numbers between 5.9 and 8,[37–43] whereas neutron diffractions (ND) yielded larger deviated values, ranging from 5.5 to 10.[37,38] With regard to the XRD and ND experiments, the ion–oxygen distances are reported between 2.39 and 2.46 Å. Although the observed difference in these experimental data is considered mainly a consequence of concentration dependence, the discrepancies in the coordination number, as well as in the ion–oxygen distance, exist even at similar concentrated solutions.[37,38,42] Recently, EXAFS measurements have demonstrated that this ion has coordination numbers between 6.8 and 8, with ion–oxygen distances between 2.43 and 2.46 Å.[17,43,44]

Apart from experiments, theoretical studies contributed even larger discrepancies. Classical simulations based on MM force fields provided large deviations in the coordination numbers, ranging from 6 to 10, with varying ion–oxygen distances between 2.39 and 2.54 Å.[29,41,45–48] In the broadest sense, the variation in results can be attributed to the use of different theoretical models. On the other hand, the inhomogeneous picture of this hydrated ion clearly indicates the important sensitivity to the applied potential functions. For quantum-mechanics-based simulations, different Car–Parrinello MD (CP–MD) simulations also gave variations in the coordination numbers of Ca^{2+} from 6 to 8, and in the ion–oxygen distance from 2.39 to 2.64 Å.[49–52] The observed difference found among CP–MD simulations has been attributed to the use of different simulation protocols and density functionals. For the treatment of electrolyte solutions, severe limitations of the CP–MD technique, in particular the use of simple generalized gradient approximations (GGA), such as Becke's exchange in conjunction with Lee–Yang–Parr's correlation functionals (BLYP) and the functionals of Perdew, Burke and Ernzerhof (PBE), combined with the relatively small system size employed in some simulations, have been well demonstrated.[27,53]

Alternatively, the QM/MM MD technique using the HF method as a benchmark has been applied for studying Ca^{2+} in water, revealing that this ion conducts coordination numbers of 8.3, with ion–oxygen distance of 2.45 Å.[31] Later on, analogous QM/MM MD simulations of Ca^{2+} in water using the HF and B3LYP methods have reported Ca^{2+} coordination numbers of 7.6 and 8.1, with corresponding ion–oxygen distances of 2.46 and 2.51 Å, respectively.[54,55] Note that the observed difference, in particular the coordination number, of two QM/MM simulations using the same HF method is not surprising, since the latter one has been performed with the use of a larger QM region. This clearly suggests that inclusion of quantum mechanical treatment beyond the first hydration shell is important in order to obtain a reliable and accurate description of this solvated ion.

In the case of Cl^{-}, the interactions of this ion with its surrounding water molecules are generally weaker than that of Ca^{2+}, and even energetically comparable with water–water interactions in bulk water. This makes the structural determination of Cl^{-} hydrate become more difficult. Consequently, the uncertainty in the coordination number of Cl^{-} in water is found both in experimental and theoretical studies, varying from 4 to 9[7,8] and from 5.1 to 8.4,[33,56–63] respectively. Previous QM/MM MD simulation of Cl^{-} in water[33] indicated that the hydration structure of this ion is quite flexible as a consequence of weak Cl^{-}-water hydrogen bonds, especially when compared to that of F^{-}. This leads to a combination of linear and bridged forms, together with a competition between the solvation of the ion and hydrogen bonding among water molecules. The QM/MM results clearly indicate the importance of QM treatment in order to correctly describe such a delicate balance between Cl^{-}–water and water–water interactions.

In the present study, the QM/MM MD simulations of Ca^{2+} and Cl^{-} in water will be revisited by using an enlarged QM region's size, together with a sufficiently long simulation period. One of the significant contributions of this study is to benchmark the performance of the QM/MM MD approach in order to generate reliable ensemble averages of such systems, from which the simulated XAS spectra are constructed and supplied in the analysis of measured XAS spectra. In addition, a set of configurations corresponding to the geometrical arrangement of the hydrated ions, as obtained from the QM/MM MD simulations, is expected to provide useful information in the process of XANES data interpretation.

2. Experimental details

2.1 XAS measurements

The experimental Ca and Cl *K*-edge XAS spectra of 2.0 M aqueous $CaCl_2$ solutions were measured at beamline 8 of Siam

Photon Laboratory, Synchrotron Light Research Institute (SLRI) in Nakhon Ratchasima, Thailand. The Siam Photon storage ring was operating at the electron energy of 1.2 GeV and the electron beam current between 80–120 mA. A Si(111) double crystal monochromator was used to select the X-ray photon energy. The solutions were kept in U-shape liquid cells with Kapton windows. All EXAFS and XANES spectra were collected at the ambient temperature and atmospheric pressure. The spectra were recorded in the transmission mode using ionization chambers as the detectors. The scanning photon energy step is set at 1 eV for the EXAFS region and 0.25 eV for the XANES region. To improve the signal-to-noise ratio, several scans were recorded and averaged. For comparison purposes, the measured XAS spectra were aligned to the corresponding spectra reported in the literature.[17,39,44]

2.2 XAS data analysis

2.2.1 EXAFS. According to the standard EXAFS data analysis,[2,7] the structure factor can be described by

$$\chi(E) = \frac{\mu(E) - \mu_0(E)}{\Delta\mu_0(E_0)}, \quad (1)$$

where $\mu(k)$ is the absorption coefficient, $E = E_0 + \hbar^2k^2/2m_e$ is the X-ray energy, $\mu_0(E)$ is the background absorption coefficient, and $\Delta\mu_0(E_0)$ is an absorption edge height. It is more common to write the structure factor as a function of the photoelectron wave vector k, $\chi(k)$. In general, $\chi(k)$ can be expressed by the classical EXAFS equation,

$$\chi(k) = \sum_j \frac{S_o^2 N_j}{k R_j^2} |f_j^{eff}(k, R_j)| \sin[2kR_j + \varphi_j(k)] e^{-2\sigma_j^2 k^2} e^{-2R_j/\lambda(k)}, \quad (2)$$

where the summation goes over all paths j, N_j is the coordination number, $S_0^2(k)$ is the amplitude reduction factor, f_j^{eff} is the curved-wave scattering amplitude, R_j is the path length, $\lambda(k)$ is the electron mean free path, $\sigma(k)$ is the Debye–Waller factor, and $\varphi(k)$ accounts for the total phase shift. Basically, if the correct geometrical configuration around the absorber atom can be obtained, the structural parameters such as path length and coordination number could be fitted with high accuracy.

To obtain the EXAFS spectra of Ca and Cl K-edge, the measured raw X-ray absorption spectra were processed using an interactive program for XAFS analysis called IFEFFIT package.[64,65] This includes (1) a background subtraction in the pre-edge and post-edge regions; (2) creating a spline curve above the threshold energy with a four-segment polynomial; and (3) extracting the oscillation by subtracting the spline from the spectra and normalizing the remaining. To enhance the EXAFS in the high k region, we choose to plot $k^2\,\chi(k)$. The plots are windowed between $2.0 < k < 8.0$ Å^{-1} using a Hanning window $W(k)$ with $dk = 1.0$ Å^{-1}.

To obtain a real-space representation of the EXAFS spectra, Fourier transformations (FT), as implemented in the IFEFFIT package, of the structural factors were carried out using

$$\tilde{\chi}(R) = \frac{1}{\sqrt{2\pi}} \int_0^\infty k^2 \chi(k) W(k) e^{i2kR} dk \quad (3)$$

Once the EXAFS spectra are processed, information on the local structure of the absorber atom can be obtained by fitting with predetermined local structure models. If all absorber atoms are expected to have the same local structure, a single local structure model can be used to fit the measured spectra with some parameters, such as the neighboring distances and coordination numbers, allowed to relax.[66] If two or more local structure models are expected, such models can be used in combination for the fit which allows more degrees of freedom.[67] For aqueous ionic solutions, however, water molecules surrounding the ions are quite labile, *i.e.*, there are uncountable forms of local structures. Consequently, the measured spectra are regarded as the statistical average of all structures.[68] Several groups have reported success in finding the proper configuration averages of ionic hydration structures with shells of water molecules.[17,21,39,44,66,68] Such models, with appropriate parameters (*i.e.*, neighboring distances and coordination numbers), can produce good fits to the experimental measurements. In this work, the structural parameters from EXAFS spectra were extracted using nonlinear least squares fitting procedure in IFEFFIT. In the fitting process, the interatomic distances (R) of each shell, coordination number, mean-square thermal, static deviation in R (σ^2), and the threshold energy (E_0) were allowed to vary. To obtain the best fit, the amplitude reduction factors (S_0^2) for Ca^{2+} and Cl^- ions were set to 0.83 and 0.91, respectively. The theoretical phase and amplitude functions were calculated using FEFF codes.[64,65,69,70] In fact, it should be noted that the neighboring distance and the coordination number of a representative structure that best fit the experimental EXAFS do not necessarily equal the average values of all structures that comprise the measured EXAFS.

2.2.2 XANES. The IFEFFIT utility program was employed to process the measured raw X-ray absorption spectra of Ca and Cl K-edge. In the XANES region, the background subtractions based on the information from the pre-edge regions are performed. Then, the XANES spectra are normalized and compared with the simulated spectra.

3. Computational details

3.1 QM/MM MD simulations

Using the QM/MM MD technique,[26–36] the system is divided into two parts, namely QM and MM regions. The total interaction energy of the system is defined as

$$E_{total} = \langle \Psi_{QM} | \hat{H} | \Psi_{QM} \rangle + E_{MM} + E_{QM-MM}, \quad (4)$$

where $\langle \Psi_{QM} | \hat{H} | \Psi_{QM} \rangle$ refers to the interactions within the QM region, while E_{MM} and E_{QM-MM} represent the interactions within the MM and between the QM and MM regions, respectively. The QM region, the most interesting part which contains the ion and its surrounding water molecules, is treated quantum mechanically, while the rest of the system is described by classical pair potentials. In practice, the total force of the system is described by the following formula:

$$F_{tot} = F_{MM}^{sys} + F(_{QM}^{QM} - F_{MM}^{QM}) \quad (5)$$

where F_{MM}^{sys}, F_{QM}^{QM}, and F_{MM}^{QM} are the MM force of the total system, the QM force in the QM region and the MM force in

the QM region, respectively. In this respect, the F_{MM}^{QM} term accounts for the coupling between the QM and MM region.

In principle, the post-HF methods with the extended basis sets are most suitable for the QM treated region but it turns out to be computationally prohibitive. With regard to this point, some essential parameters such as the level of quantum mechanics calculations, basis set and size of QM region must be optimized, compromising between the quality of the simulation results and the requirement of CPU time. Since the performance of correlated *ab initio* methods is still far too time-consuming, the Hartree–Fock (HF) method was employed for the treatment of all interactions within the QM region. The HF method has been well validated in previous QM/MM studies,[26–36] even for the treatment of anions.[33] Density functionals, such as B3LYP, are not taken into consideration since it has been demonstrated that these functionals often overestimate the ion–water interactions, which leads to a remarkably more compact and too rigid ion–water complex.[26,27] All quantum mechanical calculations were carried out using DZV+,[71] LANL2DZ,[71,72] and 6-31+G[73,74] basis sets for H_2O, Ca^{2+}, and Cl^-, respectively. The QM sizes with diameters of 8.8 and 9.2 Å were chosen for the systems of aqueous Ca^{2+} and Cl^- solutions, respectively. These QM sizes, which contain the ion and about 12–15 (for Ca^{2+}) and 11–16 (for Cl^-) water molecules, were considered large enough to ensure that the quantum mechanical forces beyond the QM region smoothly converge to pair potential forces. For the treatment of all interactions within the MM and between the QM and MM regions, a flexible model, which describes intermolecular[75] and intramolecular[76] interactions, was employed for water and the pair potential functions for describing Ca^{2+}-H_2O and Cl^--H_2O interactions were obtained from previous works.[31,33]

During the QM/MM MD simulations, exchange of water molecules between the QM and MM regions took place frequently. With regard to this point, the forces acting on each particle in the system were switched according to which region the water molecule was entering or leaving the QM region and are defined as

$$F_i = S_m(r)F_{QM} + (1-S_m(r))F_{MM}, \quad (6)$$

where F_{QM} and F_{MM} are quantum mechanical and molecular mechanical forces, respectively. $S_m(r)$ is a smoothing function[77] described by

$$\begin{aligned} S_m(r) &= 1, && \text{for } r \le r_1, \\ S_m(r) &= \frac{(r_0^2 - r^2)^2(r_0^2 + 2r^2 - 3r_1^2)}{(r_0^2 - r_1^2)^3}, && \text{for } r_1 < r \le r_0, \\ S_m(r) &= 0, && \text{for } r > r_0, \end{aligned} \quad (7)$$

where r_1 and r_0 are distances characterizing the start and end of the QM region, applied within an interval of 0.2 Å (*i.e.*, between the Ca–O and Cl–O distances of 4.2–4.4 and 4.4–4.6 Å, respectively).

In this work, the QM/MM MD simulations for aqueous Ca^{2+} and Cl^- solutions were separately performed in a canonical ensemble at 298 K with periodic boundary conditions. The system's temperature was kept constant using the Berendsen algorithm.[78] A periodic box, with a box length of 18.17 Å, contains one ion and 199 water molecules, corresponding to the experimental density of pure water. The reaction-field method[79] was employed for the treatment of long-range interactions. The Newtonian equations of motions were treated by a general predictor–corrector algorithm. The time step size was set to 0.2 fs, which allows for the explicit movement of the hydrogen atoms of water molecules. For both aqueous Ca^{2+} and Cl^- solutions, the simulations were started with the system's re-equilibration for 25 000 time steps, followed by another 250 000 (Ca^{2+}) and 100 000 (Cl^-) time steps to collect the configurations every 10th step.

3.2 Calculations of QM/MM–EXAFS and QM/MM–XANES spectra

Once the QM/MM MD simulations have been performed, sets of molecular configurations (for both aqueous Ca^{2+} and Cl^- solutions) obtained from the simulations are used to produce theoretical XAS spectra. With regard to the QM/MM MD simulations, the periodic box contains only one ion (Ca^{2+} or Cl^-) surrounded by water molecules and the time evolution of the system is studied. Since the systems of this kind are *ergodic*, we can sample the system at various times to represent the ensemble average that can be used to compare with measured XAS spectra. In this work, the QM/MM MD frames, obtained at every 0.5 ps, are sampled, from which the positions of oxygen and hydrogen atoms with respect to the central ion in each chosen frame were used to construct the QM/MM–EXAFS and QM/MM–XANES spectra. All the calculated QM/MM–EXAFS and QM/MM–XANES spectra are generated using the FEFF codes.[69,70]

For EXAFS calculations, we employed most of the default setting in the FEFF codes and restricted the scattering path to the length of 5.0 Å. In the case of XANES, the codes utilize a full multiple scattering approach based on *ab initio* overlapping muffin-tin potentials. The muffin-tin potentials were obtained using self-consistent calculations with a Hedin–Lundqvist (HL) exchange–correlation function.[80] The (time-consuming) self-consistent calculations were performed in a sphere with a radii of 5.6 Å centering on the absorbing ion. Such a sphere contains about 25–30 water molecules, which is sufficient to take into account the influence from the outer solvation shell. Test calculations show that further increasing the sphere radii leads to an exponential increase in computational time, but without a significant change on the XANES spectra. The full multiple scattering calculations include all possible paths within a larger cluster radius of 9.2 Å (consisting of 105–110 water molecules).

In addition, the established QM/MM–EXAFS spectra provide an opportunity to test how well the usual EXAFS, fitted by a model containing two shells of water molecules, can describe the systems. This can be done by simply treating the QM/MM–EXAFS spectra as experiment spectra and fitting them. After the fit, the obtained neighbor distances and the coordination numbers can be used to compare with the values obtained from the QM/MM MD analysis. In general, it should

be noted that the XAS techniques are employed to study the local structure around the absorber atoms, where there are only one or two (at most a few) different configurations in the sample. In the fitting (using a theoretical model), one generates the corresponding spectra from an assumed configuration (or the mixture of a few configurations) where the species of neighbors, number of neighbors, and neighboring distances can be varied to produce the results that fit the measured data. For aqueous ionic solutions, especially for the case where water molecules are less bounded to the ion, the situation is much more different since there are virtually infinite different configurations, *i.e.*, the ion is surrounded differently by water molecules during the measurement. Therefore, it is unexpected that a single representative shell model, as usually assumed in the EXAFS fitting, can be fitted to the spectra and represent correctly the average parameters (for instance, the coordination number). This will be discussed again in the Results section.

4. Results and discussion

4.1 QM/MM MD results

Structural properties of the hydrated Ca^{2+} and Cl^- can be explained in terms of Ca–O and Cl–O radial distribution functions (RDFs) and their corresponding integration numbers, as shown in Fig. 1. For Ca^{2+}, the first Ca–O maximum is centered at 2.45 Å, where integration up to the first minimum of the Ca–O peak yields an average coordination number of 7.4. In addition, the first solvation shell is well separated from the outer region, suggesting that first-shell water molecules are rather arranged with respect to the strong influence of Ca^{2+}. Compared to the earlier QM/MM MD work,[31] which reported a broad minimum of the first Ca–O RDF with an average number of first-shell waters of 8.3, the observed lower coordination number of Ca^{2+} could be attributed to the use of larger QM size (*i.e.*, in eqn (7) r_0 = 4.4 Å *versus* 3.6 Å used in ref. 31). A similar trend is found in the analogous QM/MM MD simulation of Ca^{2+} in water using r_0 of 4.0 Å,[54,55] which also predicted the rather well-defined first hydration shell with an average coordination number of 7.6. In this respect, it could be demonstrated that the QM treatment for the non-additive contributions beyond the first hydration shell is somewhat important in determining the hydration shell structure of Ca^{2+}. Recently, a new QM/MM framework using an *ab initio* quantum mechanical charge field (QMCF) has been applied for aqueous Ca^{2+} solutions.[81] The Ca–O distance and the coordination number were found to be 2.55 Å and 7.9, respectively. Compared to the previous QM/MM results, the observed difference in the structural properties has been demonstrated due to the use of solute–solvent potentials in the conventional QM/MM MD scheme, which probably reflect in slight artificial pressure on the primary hydration layer. In terms of CP–MD simulations, coordination numbers between 6 and 8 are reported, with observed large variations in the Ca–O distances, ranging from 2.39 to 2.64.[49–52] In most cases, the shape and width of the resulting Ca–O RDFs are rather sensitive to the density functionals applied, showing too rigid an arrangement of the hydration shell of Ca^{2+} (*i.e.*, compared to the present QM/MM MD results). Recently, it has been demonstrated that the simple density functionals BLYP and PBE usually employed in the CP–MD scheme are not even capable of describing the solvent water itself, as the use of these functionals yields a glassy state rather than a liquid at room temperature and up to 400 K.[53]

In the case of Cl^-, a less pronounced first Cl–O RDF, with a maximum at 3.24 Å, is observed. The shape and height of the first Cl–O peak clearly indicate a high flexibility of this hydrated ion. In addition, the first peak of Cl–O RDF is not distinctly separated from the bulk, which suggests an easy exchange of water molecules between the first hydration shell and the outer region. An integration up to the first Cl–O minimum leads to an average coordination number of 5.5. In fact, as a consequence of the broad Cl–O minimum, the observed coordination number of Cl^- could be regarded as a rough estimate, *i.e.*, a small shift in the position of the Cl–O minimum could lead to a significant difference in the average coordination number. For example, as can be seen in Fig. 1, the integrations up to the Cl–O distances of 3.5 and 4.0 Å yield 4.5 and 8.0 water molecules, respectively. Fig. 2 shows the arrangement of water molecules around Cl^- compared to those in the bulk water itself, as obtained by the similar

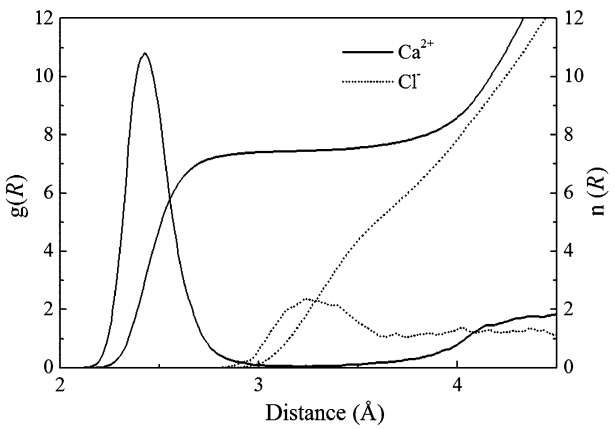

Fig. 1 Ca–O and Cl–O RDFs and their corresponding integration numbers.

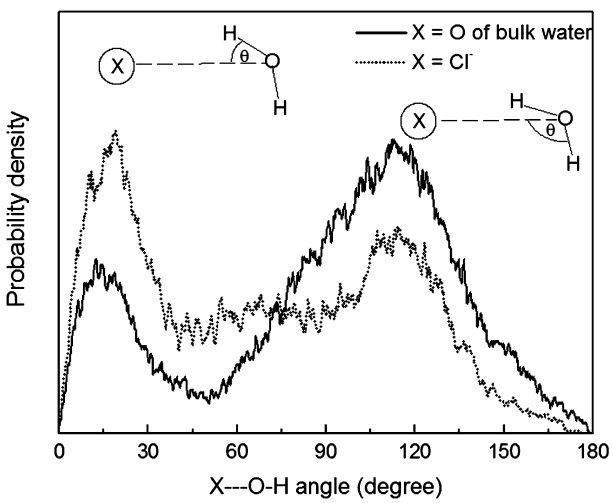

Fig. 2 Distributions of the X—O–H angle (X = O and Cl^-), calculated within the first minimum of the O–O and Cl–O RDFs.

QM/MM methodology.[82] It is obvious that water molecules in the hydration shell of Cl^- are not bound by classical hydrogen bonds to the ion. Instead, they are rather arranged with respect to a combination of linear and bridged forms. Consequently, this leads to a competition between the solvation of the ion and hydrogen bonding among water molecules. The results obtained by the present QM/MM MD simulation are in good accord with the previous QM/MM MD study,[33] which demonstrated the relative weak Cl^-–water hydrogen bonds and a high flexibility of the hydration shell structure. According to a recent CP–MD study,[83] the overestimation of ion–water hydrogen bonds is recognizable, *i.e.*, by the strong pronounced first Cl–O and Cl–H RDFs.

Fig. 3 shows probability distributions of the coordination numbers, calculated within first minimum of the Ca–O and Cl–O RDFs, respectively. For Ca^{2+}, the most frequent coordination number for this ion is 7, followed by 8 in a smaller amount. In addition, a slight distribution for the coordination number of 6 (~5%) clearly indicates lesser significance of $Ca^{2+}(H_2O)_6$ formation. In the case of Cl^-, although the 5- and 6-fold coordinated complexes are most frequently found during the QM/MM MD simulation, numerous possible species of the hydrated Cl^- exist, varying from 3 to 9. The observed large variation in the coordination numbers clearly indicates high flexibility of the hydration structure of Cl^- as well as high mobility of its first-shell water molecules. Fig. 4 displays the O–X–O angular distributions, calculated up to the first minimum of the X–O RDFs for X = Ca^{2+} and Cl^-, respectively. For Ca^{2+}, the structural arrangement of this hydrated ion with respect to the distinct coordination numbers between 7 and 8 is well reflected, *i.e.*, by the two pronounced peaks between 60–90° and between 130–150°. Unlike Ca^{2+}, the observed broad O–Cl–O peak corresponds to the numerous species of hydrated Cl^- complexes formed in aqueous solution. In fact, it should be noted that water molecules in the hydration shell of Cl^- are organized differently from that of Ca^{2+} hydration, *i.e.*, they are arranged with respect to the resultant force of the competition between the Cl^-—H–O hydrogen bonds (see Fig. 2) and the hydrogen bonding among water molecules in the same shell and/or the bulk.

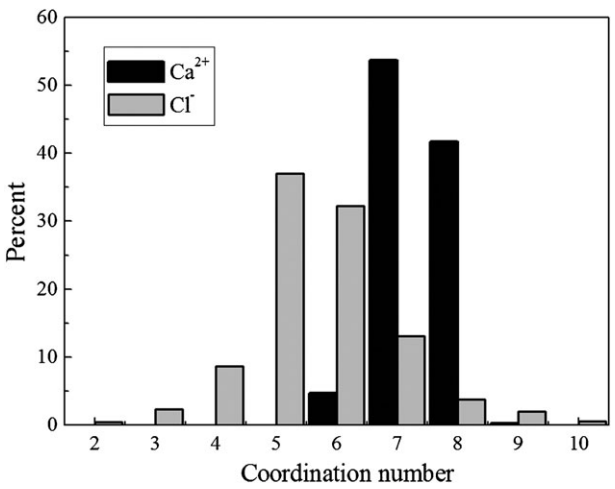

Fig. 3 Distributions of the coordination numbers of Ca^{2+} and Cl^-, calculated within the first minimum of the Ca–O and Cl–O RDFs.

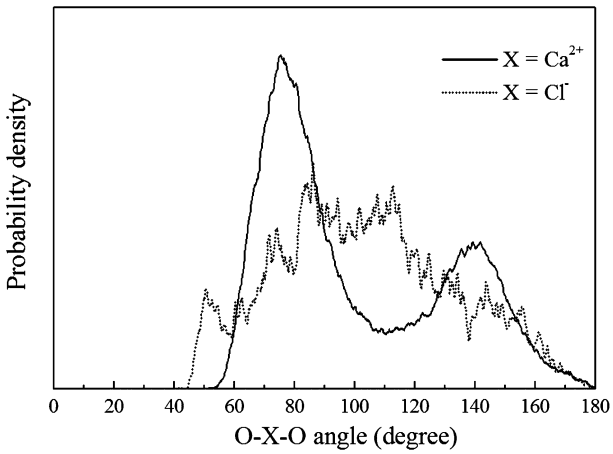

Fig. 4 Distributions of the O-X-O angle (X = Ca^{2+} and Cl^-), calculated within the first minimum of the Ca–O and Cl–O RDFs.

More detailed information on the structural arrangement of the hydrated Ca^{2+} and Cl^- complexes can be visualized through the plots of the Ca–O and Cl–O distances against the simulation times, as shown in Fig. 5 and 6, respectively. According to Fig. 5, it is obvious that the $Ca^{2+}(H_2O)_7$ and $Ca^{2+}(H_2O)_8$ complexes are dominantly formed in aqueous solution. Within a simulation time of 50 ps, only 12 water molecules are found to be involved in about 27 water exchange processes, indicating that most of the first-shell waters are tightly bound to the ion. In contrast to Ca^{2+}, water molecules surrounding Cl^- are quite labile (see Fig. 6), showing numerous water exchange processes during the QM/MM MD simulation. This clearly anticipates fast water-exchange rates of the first hydration shell, and thus shows large variations in the coordination number of this ion.[34]

4.2 EXAFS and QM/MM–EXAFS spectra

With respect to the short-range nature of XAS, this technique is suitable for studying local geometry, especially for the disordered systems. In the EXAFS region, the single back-scattering processes are mostly dominant. Making use of

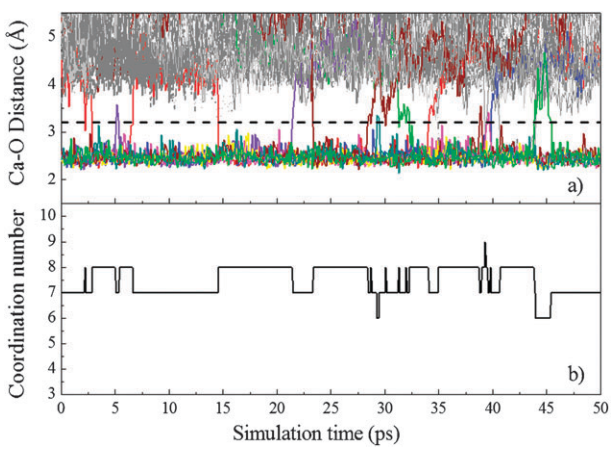

Fig. 5 Time dependences of (a) Ca^{2+}—O distance and (b) number of first-shell waters, as obtained from 50 ps of the QM/MM MD simulation. In Fig. 5a), the dash line parallel to the *x*-axis indicates the first minimum of the Ca–O RDF.

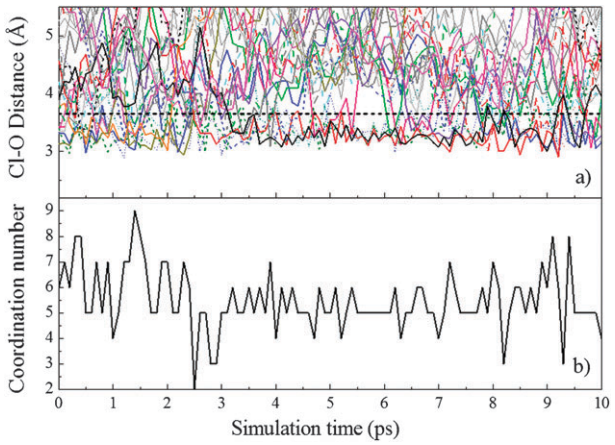

Fig. 6 Time dependences of (a) Cl^-—O distance and (b) number of first-shell waters, selecting only for first 10 ps of the QM/MM MD simulation. In Fig. 6a), the dash line parallel to the *x*-axis indicates the first minimum of the Cl–O RDF.

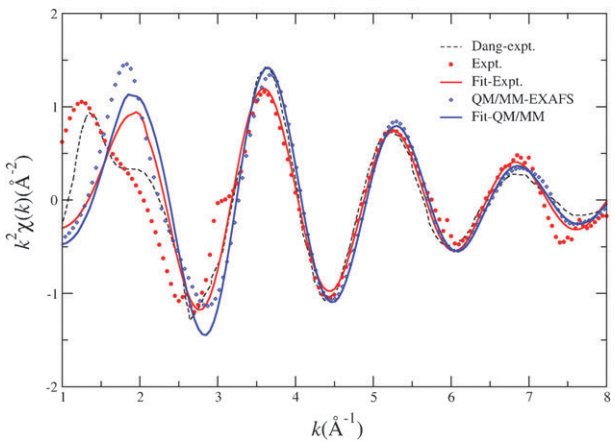

Fig. 7 Structural factors and the corresponding fitted curves for Ca^{2+} in water, as obtained from the QM/MM MD simulation and the experimental measurements.

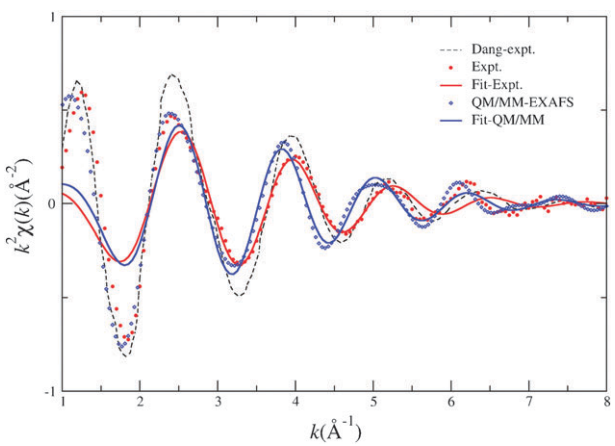

Fig. 8 Structural factors and the corresponding fitted curves for Cl^- in water, as obtained from the QM/MM MD simulation and the experimental measurements.

Table 1 Ion–oxygen distances, Debye–Waller factors and coordination numbers, as derived from the ion-O RDFs of QM/MM MD simulations and from the fitting of QM/MM–EXAFS and measured EXAFS spectra

Ion	Technique	R_0/Å	σ^2/Å^2	*N*
Ca^{2+}	QM/MM MD	2.45	—	7.4
	QM/MM–EXAFS	2.440 ± 0.009	0.011 ± 0.002	7.1 ± 0.7
	EXAFS	2.425 ± 0.013	0.010 ± 0.002	6.9 ± 0.7
		2.429 ± 0.03[a]	0.0115 ± 0.002[a]	6.8 ± 1.0[a]
Cl^-	QM/MM MD	3.24	—	5.5
	QM/MM–EXAFS	3.200 ± 0.034	0.026 ± 0.007	5.1 ± 1.3
	EXAFS	3.047 ± 0.040	0.032 ± 0.008	6.0 ± 1.7
		3.110 ± 0.03[a]	0.0290 ± 0.004[a]	6.4 ± 1.0[a]

[a] EXAFS measurements from Dang *et al.*[17]

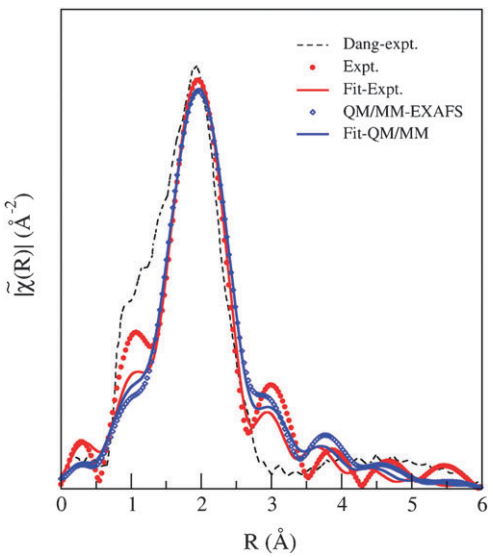

Fig. 9 Fourier transformations of the structural factors and the corresponding fitted curves for Ca^{2+} in water, as obtained from the QM/MM MD simulation and the experimental measurements.

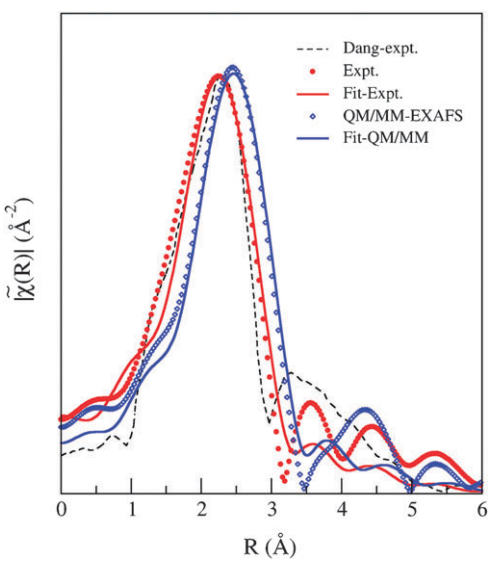

Fig. 10 Fourier transformations of the structural factors and the corresponding fitted curves for Cl^- in water, as obtained from the QM/MM MD simulation and the experimental measurements.

combined QM/MM MD simulations and the EXAFS measurements technique, however, it should be realized that the measured XAS spectra of ions in aqueous solution (where there are virtually infinite different configurations) may not necessarily be well fitted by one configuration model. Even if there is a configuration model that can fit the spectra well, the result obtained from the model might not represent the average of all configurations in the sample.

In this work, the QM/MM MD technique is expected to be an elegant simulation approach in order to generate reliable QM/MM–EXAFS spectra. The QM/MM–EXAFS spectra are generated by averaging 30 snapshot frames of the QM/MM MD simulations. (Test calculations show that increasing the snapshot frames does not significantly change the averaged spectra.) In this respect, it is worth noting that all major structural details of the ion–water structures inherent in the simulations are mutually represented in the QM/MM–EXAFS spectra. The QM/MM–EXAFS spectra are also fitted with respect to classical EXAFS in eqn (2). The general reason is to gauge how well the nearest neighbor distance and the coordination number, as obtained from the simulated EXAFS spectra, fit a single configuration resembling the values determined from the analysis of the full QM/MM MD data.

Fig. 7 and 8 show the k^2-weighted $\chi(k)$ spectra for Ca^{2+} and Cl^- in water, respectively, comparing between the QM/MM–EXAFS and the experimental measurements along with their corresponding fits. For the EXAFS spectra, the data measured by Dang *et al.*[17] were also given for comparison. For Ca^{2+} (Fig. 7), the oscillation periods of the measured EXAFS and the QM/MM–EXAFS spectra are in good agreement,

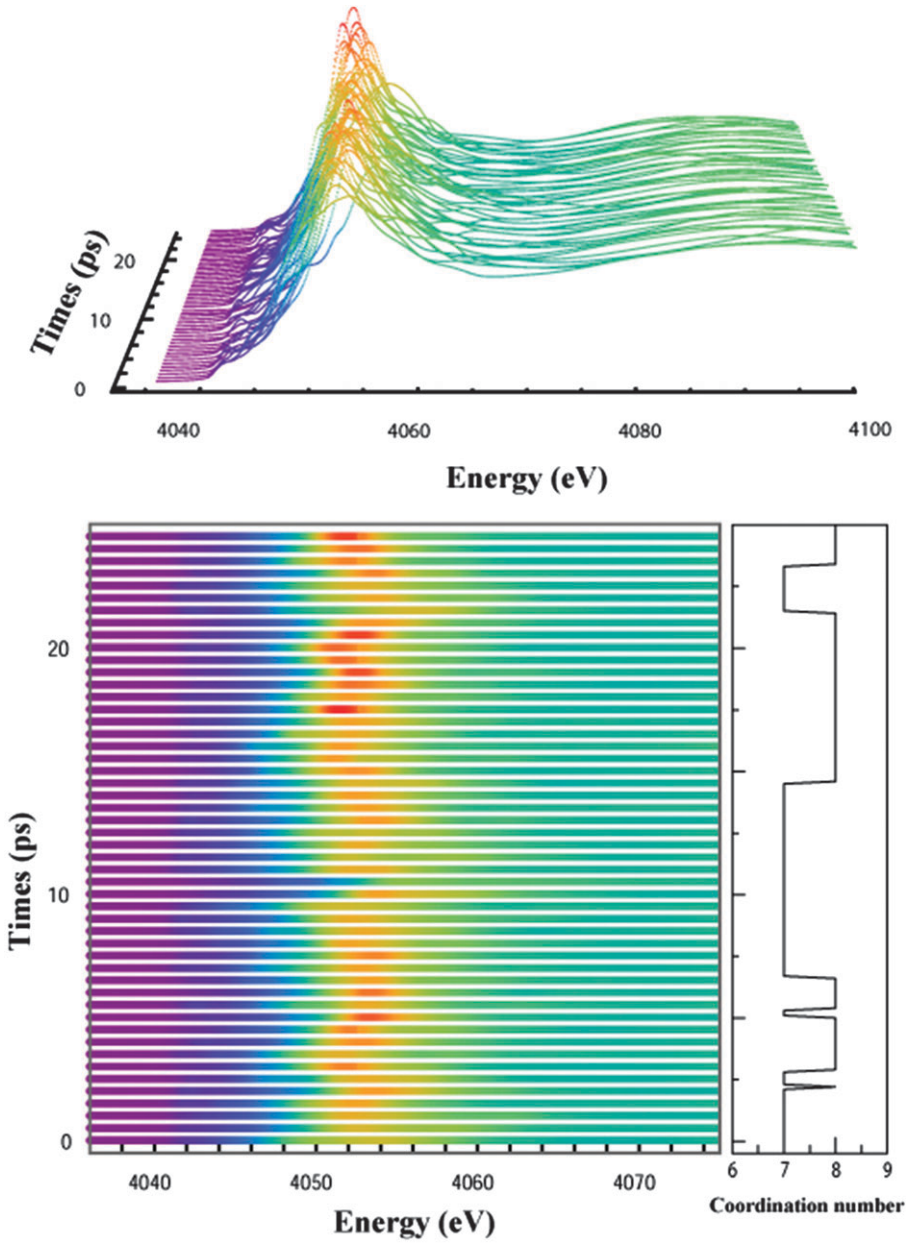

Fig. 11 Examples of the simulated QM/MM–XANES spectra for Ca^{2+} in water.

i.e., implying good accordance in the average Ca–O distances. The observed disagreement in the low k region between the QM/MM–EXAFS and the measured EXAFS spectra (this work and Dang *et al.*) can be described due to the residue of a different atomic background subtraction and treatment of anomalous features in the EXAFS signal processing steps. In addition, this region of the spectra belongs to the XANES region, in which the algorithm employed cannot generate accurate EXAFS spectra. In the case of Cl^- (Fig. 8), the observed discrepancy between our experimental $\chi(k)$ spectrum and that measured by Dang *et al.* becomes more apparent, compared to that of the aqueous Ca^{2+} system. This can be explained by the high noise level of our measurement due to a low photon flux as well as strong water absorption at Cl^- K-edge region (2800–3000 eV). With regard to the present EXAFS data, the noise level of the spectrum remains actually the same throughout the spectrum. However, the signal decays rapidly at high k, leading to a higher signal-to-noise ratio. In addition, since the plot is k^2-weighted, the noise is also significantly amplified. In this study, the QM/MM–EXAFS spectrum shows fair agreement in the oscillation periods when compared to the curves measured by experiments.

Following the expression given by eqn (2), the theoretical fit based on a single configuration is applied to the measured EXAFS and simulated QM/MM–EXAFS spectra. Some essential parameters for both Ca^{2+} and Cl^- systems are summarized in Table 1. In comparison to the data by Dang *et al.*,[17] good agreement in the fitting results is visible, especially for the case of Ca^{2+}. In addition, the parameters R_0 and N derived from the analysis of the QM/MM MD simulation (average overall ensemble) are in good accord with the values obtained from the fit of the QM/MM–EXAFS spectra. For Ca^{2+}, the structural parameters obtained from the fit are in good agreement with the analysis of the simulation data (Table 1). This is not surprising because most of the frames used for generating the QM/MM–EXAFS spectra are expected to have similar local hydration structures due to the tight binding of the first hydration shell. In contrast to Ca^{2+}, the observed larger variation in the fitting results could be ascribed to the rather weak Cl^--water interactions, which lead to high flexibility of this ion hydrate. As a result, the QM/MM–EXAFS spectra are constructed with respect to the frames that are distinctive in the hydration shell structures. Thus, they are not expected to fit well by a single configuration in the EXAFS equation. On the other hand, the fitting process forces a configuration that gives an overall feature in the best agreement with the average spectrum obtained from distinctive frames. However, as mentioned previously, the configuration obtained from the fit does not necessarily represent the average of all ion configurations in the sample. For both Ca^{2+} and Cl^- systems, our results show that the configurations obtained from the fits of QM/MM–EXAFS spectra can provide data in good accord with the average values derived from the simulated ensembles. Overall, it could be demonstrated that, for a tightly bound hydration structure like Ca^{2+}, the EXAFS fit can yield the configuration that well represents the average of the ensemble. For more labile hydration structures like Cl^-, however, the EXAFS fit may not be able to precisely represent the average of the ensemble as a consequence of numerous possible species of the hydrated Cl^- found in aqueous solution.

The Fourier transformations (eqn (3)) of the QM/MM–EXAFS and the corresponding measured EXAFS spectra yield the real space distribution plots, as shown in Fig. 9 and 10 for the aqueous Ca^{2+} and Cl^- solutions, respectively. The main peak of the $\tilde{\chi}(R)$ spectra is primarily corresponding to the scattering originated from the oxygen atoms of first-shell water molecules. For Ca^{2+} systems, the peak position and shape obtained from the QM/MM–EXAFS spectrum are in good accord with the experimental measurements. For the Cl^- system, the peak position obtained from the QM/MM–EXAFS spectrum is exhibited at a slightly larger distance, compared to the experimental measurements. This can be ascribed due partly to the neglect of the electron correlation in the HF calculations, which generally diminishes the Cl^-–water interactions.

4.3 XANES and QM/MM–XANES spectra

In the XANES region, since the kinetic energy of the photoelectron is low, the excited electron density of states plays a dominant role. In order to obtain the correct partial density of states, detailed atomic potentials have to be correctly calculated and an extensive MS approach has been used. For the case of aqueous Ca^{2+} and Cl^- solutions, the densities of states are strongly sensitive to the detailed arrangement of water molecules surrounding the ions. In general, XANES spectra are considered to be insensitive to long-range disorder, but related to characteristics of the geometrical arrangement of the hydrated ions. Consequently, these spectra are often used as fingerprint for characterizing the neighborhood of the ions. For Ca^{2+}, examples of the XANES spectra generated from every 0.5 ps of the QM/MM MD snapshots are plotted in Fig. 11. Obviously, each QM/MM–XANES spectrum generated from each QM/MM MD snapshot, which corresponds to a different hydration structure of Ca^{2+}, is different. This confirms that each of the QM/MM–XANES spectra is sensitive

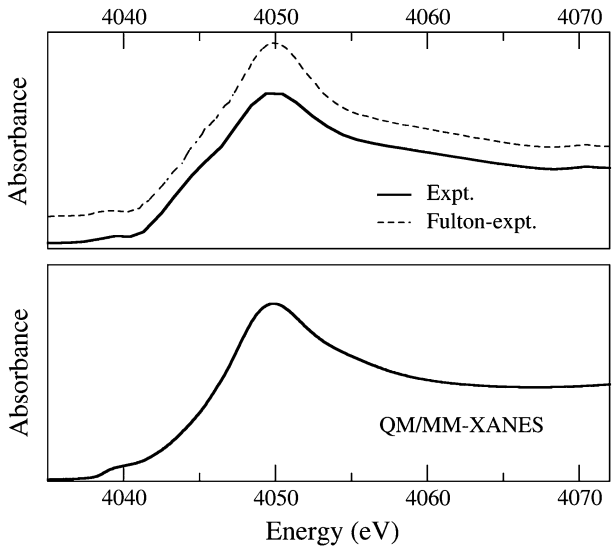

Fig. 12 Comparison between the experimental Ca K-edge XANES spectra and the averaged QM/MM–XANES spectrum.

to the details of the hydration structure around the ion. A comparison between the measured and the average QM/MM–XANES spectra is shown in Fig. 12. For the experimental data, the spectrum measured by Fulton *et al.*[84] was also given for comparison. It should be noted that, in principle, the representative set of hydration structures used for generating the average QM/MM–XANES spectrum has to be extracted with proper statistics from the QM/MM MD trajectories that cover all possible configurations. In this work, the set of snapshots is taken from the QM/MM MD simulation of a time-scale that is sufficient to provide a reliable ensemble average. As can be seen in Fig. 12, despite the observed difference among the isolated QM/MM–XANES spectra obtained from each of the QM/MM MD snapshots, the average QM/MM–XANES spectrum gives satisfactory agreement with the measured XANES spectra.

For the case of Cl^-, examples of the simulated XANES spectra with respect to each of 0.5 ps QM/MM MD snapshots are shown in Fig. 13. The average QM/MM–XANES spectrum is plotted and compared to the corresponding XANES measurements, as depicted in Fig. 14. According to the high flexibility (less defined) of the Cl^- hydrate, the distinction among the XANES from each snapshot becomes more prominent as compared to the Ca^{2+} case. In this respect, the statistical information regarding all possible hydration shell structures from the QM/MM MD simulation has an even more important effect on the average spectrum. As can be seen in Fig. 14, it is clear that the main features in the average XANES spectrum show good agreement with the experimental ones. This clearly indicates that the geometrical arrangements of the hydrated Cl^- obtained by the QM/MM MD simulation are realistic.

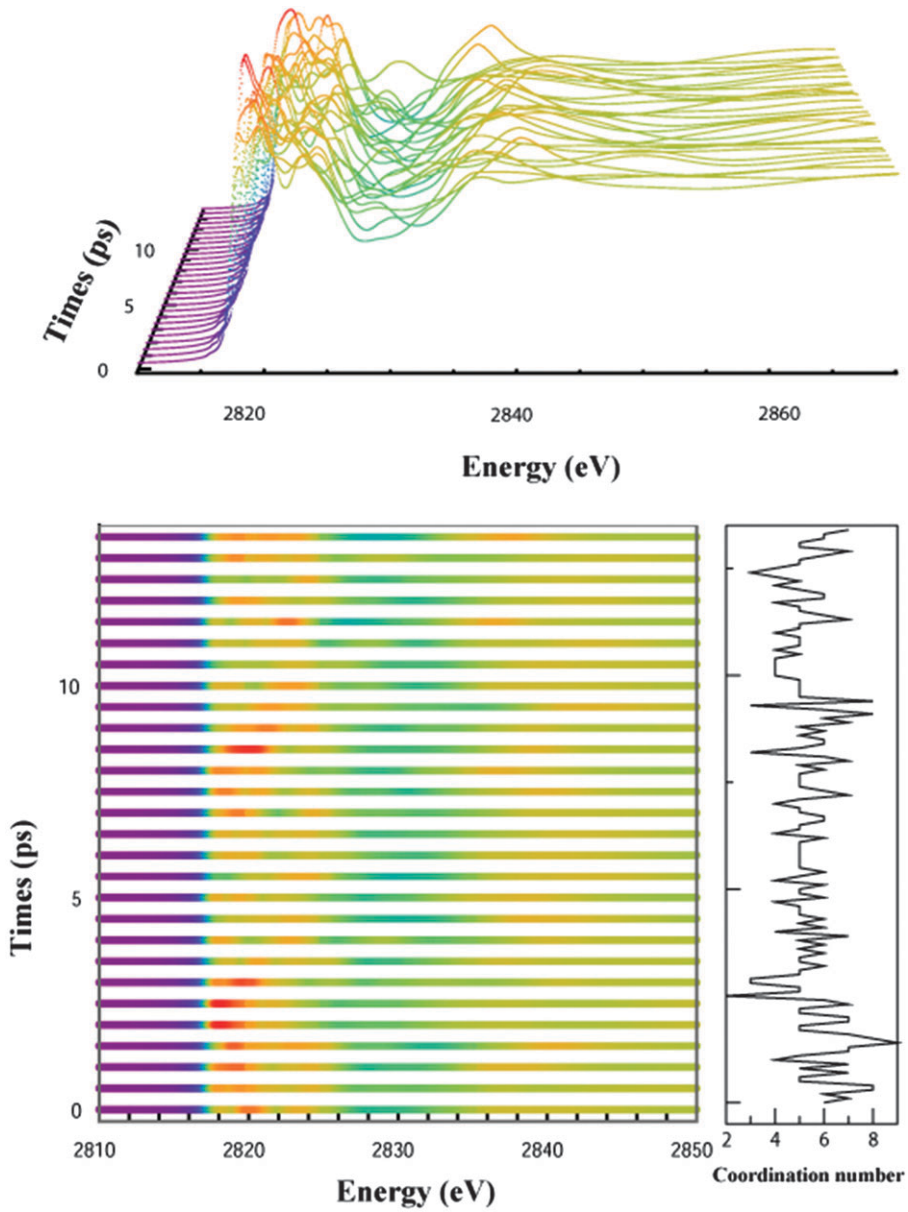

Fig. 13 Examples of the simulated QM/MM–XANES spectra for Cl^- in water.

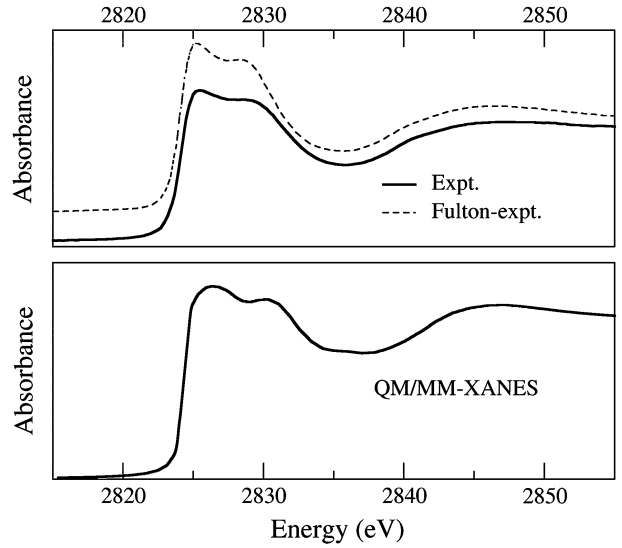

Fig. 14 Comparison between the experimental Cl *K*-edge XANES spectra and the averaged QM/MM–XANES spectrum.

Because the equally spaced (in time) snapshots are obtained from the QM/MM MD simulation without bias or any fitting to the experimental XANES, this agreement supplies information that the trajectory derived from the QM/MM MD simulation can realistically represent the actual system. This illustrates that the fact for an *ergodic* system, like the case at hand, we can calculate a temporal average XANES spectrum by choosing a sufficiently large number of equally spaced (in time) snapshots and compare with the measured spectrum which represent both the temporal and ensemble average. The agreement confirms that the overall simulation, *i.e.*, both the dynamic behavior and the static details of each snapshot, is consistent with reality. With regard to this point, if the dynamics details obtained from the simulation are wrong, the resulting average XANES spectrum would be dominated by the feature of the wrong configuration and would not agree with that of the experiments. In this context, the molecular configurations obtained by the QM/MM MD simulation can be used as reliable representatives for the geometrical arrangement of the Ca^{2+} and Cl^{-} hydrations.

5. Conclusions

In this work, we combine the QM/MM MD technique with the XAS measurements for studying the hydration shell structures of Ca^{2+} and Cl^{-}. The QM/MM MD results and the detailed analysis on the measured XAS spectra clearly indicate the characteristically low symmetry and disordered nature of the first coordination shell of these ions, especially for the case of Cl^{-}. In terms of XAS measurements, the presence of MS effects in the measured spectra and the errors from asymmetric distributions are the major problems in the analysis of XAS data. To simplify these problems, QM/MM MD simulations have been performed to generate theoretical XAS spectra, from which these spectra have been used as starting models in the XAS data analysis. Since the accuracy in the interpretation of XAS data depends crucially on the reliability of the simulated XAS models, the use of a more sophisticated QM/MM MD technique is highly recommended over other MM approaches in order to generate a reliable ensemble average, *i.e.*, a better theoretical $\chi(k)$. In particular for XANES, since there is no direct relationship between the XANES spectrum and the dynamic details relating to the geometrical arrangement of the hydrated ion, a representative set of geometries extracted from the QM/MM MD trajectories is extremely useful in order to simplify the process of XANES data interpretation.

Acknowledgements

This work was supported by the Thailand Research Fund (TRF, Grant No. RTA5280009). The corresponding author also acknowledges support from the Synchrotron Light Research Institute (SLRI) and TRF (Grant No. BRG5180018).

References

1 H. Frank, in *Chemical Physics of Ionic Solutions*, John Wiley & Sons, New York, 1956.
2 R. J. P. Williams, in *Bio-inorganic Chemistry*, American Chemical Society, Washington DC, 1971.
3 J. E. Enderby and G. W. Neilson, *Rep. Prog. Phys.*, 1981, **44**, 593.
4 I. Howell and G. W. Neilson, *J. Phys.: Condens. Matter*, 1996, **8**, 4455.
5 M. Magini, G. Licheri, G. Paschina and G. Piccaluga, in *X-ray Diffraction of Ions in Aqueous Solutions: Hydration and Complex Formation*, CRC Press, Boca Raton, 1988.
6 G. W. Neilson, *Pure Appl. Chem.*, 1988, **60**, 1797.
7 G. W. Neilson and R. H. Tromp, *Annu. Rep. Prog. Chem., Sect. C*, 1991, **88**, 45.
8 H. Ohtaki and T. Radnai, *Chem. Rev.*, 1993, **93**, 1157.
9 N. T. Skipper, G. W. Neilson and S. C. Cummings, *J. Phys.: Condens. Matter*, 1989, **1**, 3489.
10 D. E. Crozier, J. J. Rehr and R. Ingalls, in *X-ray Absorption: Principles, Applications, Techniques of EXAFS, SEXAFS and XANES*, Wiley, New York, 1988, ch. 9.
11 P. D'Angelo, A. Di Nola, A. Filipponi, N. V. Pavel and D. Roccatano, *J. Chem. Phys.*, 1994, **100**, 985.
12 D. E. Crozier, *Physica B*, 1995, **208–209**, 330.
13 D. E. Crozier, *Nucl. Instrum. Methods Phys. Res., Sect. B*, 1997, **133**, 134.
14 P. D'Angelo, A. Di Nola, E. Giglio, M. Mangoni and N. V. Pavel, *J. Phys. Chem.*, 1995, **99**, 5471.
15 P. D'Angelo and N. V. Pavel, *J. Chem. Phys.*, 1999, **111**, 5107.
16 P. D'Angelo and N. V. Pavel, *J. Synchrotron Radiat.*, 2001, **8**, 173.
17 L. X. Dang, G. K. Schenter, V.-A. Glezakou and J. L. Fulton, *J. Phys. Chem. B*, 2006, **110**, 23644.
18 A. Di Cicco, *J. Phys.: Condens. Matter*, 1996, **8**, 9341.
19 A. Di Cicco, M. J. Rosolen, R. Marassi, R. Tossici, A. Fillipponi and J. Rybicki, *J. Phys.: Condens. Matter*, 1996, **8**, 10779.
20 A. Di Cicco, M. Taglienti, M. Minicucci and A. Filipponi, *Phys. Rev. B: Condens. Matter Mater. Phys.*, 2000, **62**, 12001.
21 J. L. Fulton, M. M. Hoffmann, J. G. Darab, B. J. Palmer and E. A. Stern, *J. Phys. Chem. A*, 2000, **104**, 11651.
22 A. Kuzmin, S. Obst and J. Purans, *J. Phys.: Condens. Matter*, 1997, **9**, 10065.
23 S. Rossano, A. Ramos, J.-M. Delaye, A. Filipponi, C. Brouder and G. Calas, *J. Synchrotron Radiat.*, 1999, **6**, 247.
24 A. Trapananti, A. Di Cicco and M. Minicucci, *Phys. Rev. B: Condens. Matter Mater. Phys.*, 2002, **66**, 014202.
25 S. L. Wallen, B. J. Palmer and J. L. Fulton, *J. Chem. Phys.*, 1998, **108**, 4039.
26 B. M. Rode, C. F. Schwenk, T. S. Hofer and B. R. Randolf, *Coord. Chem. Rev.*, 2005, **249**, 2993.
27 B. M. Rode, C. F. Schwenk and A. Tongraar, *J. Mol. Liq.*, 2004, **110**, 105.

28 P. Intharathep, A. Tongraar and K. Sagarik, *J. Comput. Chem.*, 2005, **26**, 1329.
29 T. Kerdcharoen, K. R. Liedl and B. M. Rode, *Chem. Phys.*, 1996, **211**, 313.
30 A. Payaka, A. Tongraar and B. M. Rode, *J. Phys. Chem. A*, 2009, **113**, 3291.
31 A. Tongraar, K. R. Liedl and B. M. Rode, *J. Phys. Chem. A*, 1997, **101**, 6299.
32 A. Tongraar, K. R. Liedl and B. M. Rode, *J. Phys. Chem. A*, 1998, **102**, 10340.
33 A. Tongraar and B. M. Rode, *Phys. Chem. Chem. Phys.*, 2003, **5**, 357.
34 A. Tongraar and B. M. Rode, *Chem. Phys. Lett.*, 2005, **403**, 314.
35 A. Tongraar, K. Sagarik and B. M. Rode, *Phys. Chem. Chem. Phys.*, 2002, **4**, 628.
36 D. Xenides, B. R. Randolf and B. M. Rode, *J. Chem. Phys.*, 2005, **122**, 174506.
37 S. Cummings, J. E. Enderby and R. A. Howe, *J. Phys. C: Solid State Phys.*, 1980, **13**, 1.
38 N. A. Hewish, G. W. Neilson and J. E. Enderby, *Nature*, 1982, **297**, 138.
39 F. Jalilevand, D. Spangberg, P. Lindqvist-Reis, K. Hermansson, I. Persson and M. Sandström, *J. Am. Chem. Soc.*, 2001, **123**, 431.
40 G. Licheri, G. Piccaluga and P. Pinna, *J. Chem. Phys.*, 1976, **64**, 2437.
41 M. M. Probst, T. Radnai, K. Heinzinger, P. Bopp and B. M. Rode, *J. Phys. Chem.*, 1985, **89**, 753.
42 P. Smirnov, M. Yamagami, H. Wakita and T. Yamaguchi, *J. Mol. Liq.*, 1997, **73–74**, 305.
43 D. Spangberg, K. Hermansson, P. Lindqvist-Reis, F. Jalilevand, M. Sandström and I. Persson, *J. Phys. Chem. B*, 2000, **104**, 10467.
44 J. L. Fulton, M. S. Heald, Y. S. Badyal and J. M. Simonsom, *J. Phys. Chem. A*, 2003, **107**, 4688.
45 F. M. Floris, M. Persico, A. Tani and J. Thomasi, *Chem. Phys. Lett.*, 1994, **227**, 126.
46 S. G. Kalko, G. Sesé and J. A. Padro, *J. Chem. Phys.*, 1996, **104**, 9578.
47 S. Obst and H. Bradaczek, *J. Phys. Chem.*, 1996, **100**, 15677.
48 G. Pálinkás and K. Heinzinger, *Chem. Phys. Lett.*, 1986, **126**, 251.
49 I. Bakó, J. Hutter and G. Pálinkás, *J. Chem. Phys.*, 2002, **117**, 9838.
50 M. M. Naor, K. V. Nostrand and C. Dellago, *Chem. Phys. Lett.*, 2003, **369**, 159.
51 F. C. Lightstone, E. Schwegler, M. Allesch, F. Gygi and G. Galli, *ChemPhysChem*, 2005, **6**, 1745.
52 T. Todorova, P. Hűnenberger and J. Hutter, *J. Chem. Theory Comput.*, 2008, **4**, 779.
53 S. Yoo, X. C. Zeng and S. S. Xantheas, *J. Chem. Phys.*, 2009, **130**, 221102.
54 C. F. Schwenk, H. Loeffler and B. M. Rode, *J. Chem. Phys.*, 2001, **115**, 10808.
55 C. F. Schwenk and B. M. Rode, *Pure Appl. Chem.*, 2004, **76**, 37.
56 J. Chandrasekhar, D. C. Spellmayer and W. L. Jorgensen, *J. Am. Chem. Soc.*, 1984, **106**, 903.
57 E. Clementi, R. Barsotti, J. Fromm and R. O. Watts, *Theor. Chim. Acta*, 1976, **43**, 101.
58 K. Heinzinger, *Pure Appl. Chem.*, 1985, **57**, 1031.
59 A. Ignaczak, J. A. N. F. Gomes and M. N. D. S. Cordeiro, *Electrochim. Acta*, 1999, **45**, 659.
60 R. W. Impey, P. A. Madden and I. R. McDonald, *J. Phys. Chem.*, 1983, **87**, 5071.
61 S. Koneshan, J. C. Rasaiah, R. M. Lynden-Bell and S. H. Lee, *J. Phys. Chem. B*, 1998, **102**, 4193.
62 M. Mezei and D. L. Beveridge, *J. Chem. Phys.*, 1981, **74**, 6902.
63 D. E. Smith and L. X. Dang, *J. Chem. Phys.*, 1994, **101**, 7873.
64 M. Newville, B. Ravel, D. Haskel, J. J. Rehr, E. A. Stern and Y. Yacoby, *Phys. B*, 1995, **208–209**, 154.
65 J. J. Rehr, R. C. Albers and S. I. Zabinsky, *Phys. Rev. Lett.*, 1992, **69**, 3397.
66 P. J. Merkling, A. Munoz-Paez and E. Sanchez Marcos, *J. Am. Chem. Soc.*, 2002, **124**, 10911.
67 P. Wernet, D. Nordlund, U. Bergmann, M. Cavalleri, M. Odelius, H. Ogasawara, L. A. Naslund, T. K. Hirsch, L. Ojamae, P. Glatzel, L. G. M. Pettersson and A. Nilsson, *Science*, 2004, **304**, 995.
68 P. D'Angelo, O. M. Roscioni, G. Chillemi, S. Della Longa and M. Benfatto, *J. Am. Chem. Soc.*, 2006, **128**, 1853.
69 A. L. Ankudinov, C. E. Bouldin, J. J. Rehr, J. Sims and H. Hung, *Phys. Rev. B: Condens. Matter Mater. Phys.*, 2002, **65**, 104107.
70 A. L. Ankudinov, B. Ravel, J. J. Rehr and S. D. Conradson, *Phys. Rev. B: Condens. Matter Mater. Phys.*, 1998, **58**, 7565.
71 T. H. Dunning and P. J. Hay, in *Modern Theoretical Chemistry*, Plenum, New York, 1976.
72 P. J. Hay and W. R. Wadt, *J. Chem. Phys.*, 1985, **82**, 270.
73 M. J. Frisch, J. A. Pople and J. S. Binkley, *J. Chem. Phys.*, 1984, **80**, 3265.
74 W. J. Hehre, R. Ditchfield and J. A. Pople, *J. Chem. Phys.*, 1972, **56**, 2257.
75 F. H. Stillinger and A. Rahman, *J. Chem. Phys.*, 1978, **68**, 666.
76 P. Bopp, G. Jancsó and K. Heinzinger, *Chem. Phys. Lett.*, 1983, **98**, 129.
77 B. R. Brooks, R. E. Bruccoleri, B. D. Olafson, D. J. States, S. Swaminathan and M. Karplus, *J. Comput. Chem.*, 1983, **4**, 187.
78 H. J. C. Berendsen, J. P. M. Postma, W. F. van Gunsteren, A. DiNola and J. R. Haak, *J. Chem. Phys.*, 1984, **81**, 3684.
79 D. J. Adams, E. H. Adams and G. J. Hills, *Mol. Phys.*, 1979, **38**, 387.
80 L. Hedin and S. Lundqvist, *Solid State Phys.*, 1970, **23**, 1.
81 L. H. V. Lim, A. B. Pribil, A. E. Ellmerer, B. R. Randolf and B. M. Rode, *J. Comput. Chem.*, 2010, **31**, 1195.
82 A. Tongraar, P. Tangkawanwanit and B. M. Rode, *J. Phys. Chem. A*, 2006, **110**, 12918.
83 J. M. Heuft and E. J. Meijer, *J. Chem. Phys.*, 2003, **119**, 11788.
84 J. L. Fulton, Y. Chen, S. M. Heald and M. Balasubramanian, *J. Chem. Phys.*, 2006, **125**, 94507.